Nuclear Instruments and Methods in Physics Research B80/81 (1993) 1356-1361
North-Holland

NIM B
Beam Interactions with Materials & Atoms

Synthesis and properties of microlaminate structures by ion beam assisted deposition

G.S. Was, J.W. Jones, C.E. Kalnas, L.J. Parfitt and A. Mashayekhi
The University of Michigan, Ann Arbor, MI 48109, USA

D.W. Hoffman
Research Staff, Ford Motor Company, Dearborn, MI 48124, USA

Films of Al, Al_2O_3, Mo and $MoSi_x$ were formed by ion beam assisted deposition (IBAD) at R ratios between 0.004 and 0.1 and film thicknesses between 150 and 1100 nm. Al films were crystalline with a strong (111) fiber texture becoming more pronounced and azimuthally oriented with increasing R ratio. Mo films were crystalline with strong (110) texture and a distinct azimuthal texture indicative of planar channeling of the ion beam along (110) planes. The microstructure of Al films is characterized by large columnar grains at $R = 0$ with breakup starting at $R = 0.04$, while that of Mo films showed little change with increasing R ratio. Al_2O_3 and $MoSi_x$ films are amorphous under all deposition conditions. The average stress in oxide and silicide films is tensile at $R = 0$ and becomes compressive with increased values of the normalized energy, saturating at ~ 15 eV/atom. The average stress in Mo films is tensile at $R = 0$, increases to a maximum value of 0.63 GPa and becomes compressive with increasing normalized energy.

1. Introduction

Microlaminates have received considerable attention in recent years because of the potential to tailor composition, microstructure and interface properties to enhance strength, toughness and oxidation resistance. Substantial increases in strength, for example, have been reported for Al/Al_2O_3 [1] and Cu/Ni [2] when layer thicknesses were less than 500 nm. In high temperature $MoSi_2$-based composites, alloying with Nb has been shown to significantly increase toughness [3], an inherent problem with silicides. While vapor deposition has traditionally been used to produce microlaminates, it has been recognized that significant improvement in properties of films can be achieved by ion beam assisted deposition (IBAD). IBAD has been shown to increase film density, promote equiaxed grain formation and film/substrate adherence, and provide control over crystal texture and residual stress [4]. The objective of this research is to synthesize Al/Al_2O_3 and $Mo/MoSi_2$ microlaminates by IBAD with the intent of developing an understanding of the dependence of microstructural and geometric variables on strength and fracture resistance. The work reported here describes the synthesis and characterization of monolithic Al_2O_3, pure Al metal films and $Mo/MoSi_x$ microlaminates produced by ion beam assisted deposition.

2. Experiment

Ion beam assisted deposition was conducted in a chamber containing two 6 kW electron beam guns and a 3 cm Kaufman ion gun with a base pressure of 2×10^{-9} Torr for 200 and 1000 nm thick Al_2O_3 films and $Mo/MoSi_x$ films, or 2×10^{-7} Torr for 150 and 400 nm thick Al_2O_3 films. Depositions were normal to the substrate at the following rates: Al: 0.7 nm/s, Al_2O_3: 1.0 nm/s, Mo: 0.25 nm/s, and $MoSi_x$: 0.25 nm/s for Mo and 0.65 nm/s for Si. Ion bombardment was performed using 209 to 593 eV Ar^+ ions at an angle of 45° to the substrate normal, with current densities in the range 2 to 190 $\mu A/cm^2$, giving a range of R (ion/atom arrival rate) ratios from 0.004 to 0.1, table 1. Results are also expressed in terms of the normalized energy, E_n, which is the product of the beam voltage and the R ratio. The chamber pressure during deposition was $1-3 \times 10^{-5}$ Torr. Deposition rates for each source were measured independently with quartz crystal monitors and the beam current was monitored with a Faraday cup. Deposited films ranged in thickness from 150 to 1100 nm.

The amount of material deposited and the composition or stoichiometry of the films deposited onto graphite foil were determined by Rutherford backscattering analysis at an angle of 165°, and fit with the aid of the program, RUMP [5]. Crystallinity and texture

Table 1
Deposition parameters and composition analysis of IBAD films

Film type	Nominal thickness [nm]	R ratio [ion/atom]	Energy [eV/ion]	E_n [eV/atom]	O/Al or Mo/Si (±0.01)	Ar [at.%] (±0.02)	O [at.%] (±0.1)
Al_2O_3	150	0	0	0	1.61	0	–
		0.004	320	1.44	1.56	0.47	–
		0.01	281	2.81	1.52	0.47	–
		0.04	400	16.0	1.50	3.08	–
		0.068	560	38.1	1.52	2.93	–
		0.1	587	58.7	1.47	4.03	–
	200	0	0	0	1.67	0	–
		0.01	380	3.8	1.49	0.99	–
		0.1	593	59.3	1.47	4.12	–
	400	0	0	0	1.67	0	–
		0.0045	320	1.44	1.53	0.65	–
		0.01	281	3.7	1.53	1.19	–
		0.04	400	16.0	1.50	2.96	–
	1000	0	0	0	1.33	0	–
		0.004	209	0.84	1.41	0.62	–
		0.04	500	20.0	1.33	0.5	–
		0.1	593	59.3	1.53	4.31	–
Al	1000	0	0	0	–	0	6.1
		0.004	250	1	–	0.47	3.8
		0.04	488	19.5	–	5.48	3.2
		0.1	463	46.3	–	4.17	3.1
Mo	200	0	0	0	–	0	17.0
		0.01	251	2.5	–	0.69	12.2
		0.025	340	8.5	–	1.0	14.9
		0.05	376	18.8	–	0.87	9.0
		0.075	409	30.7	–	1.0	6.6
		0.10	461	46.1	–	1.0	5.1
$MoSi_x$	200	0	0	0	1.35	0	3.8
		0.01	345	3.5	1.36	0.75	4.6
		0.025	415	10.4	1.37	1.43	3.8
		0.05	471	23.6	1.34	2.58	2.9
		0.075	488	36.6	1.27	3.49	2.4
		0.10	516	51.6	1.21	4.94	2.4

were determined by X-ray diffraction (XRD) using Cu K_α radiation in a Rigaku diffractometer operated at 40 kV and 100 mA. $\theta/2\theta$ scans of rotating samples were conducted for both Al and Al_2O_3 films of thickness 1000 nm. Pole figures were generated for the Al (111), (200) and (220) poles. $\theta/2\theta$ scans of rotating samples were conducted for Mo films of thickness 1000 nm and pole figures were generated for the (110) pole. Grain size and morphology were determined from transmission electron microscopy (TEM) of planar and cross section samples on a JEOL 2000 FX TEMSCAN at 200 kV. Residual stress was determined by optical interferometry [6] on 150–400 nm films of Al_2O_3, 200 nm films of Mo and $MoSi_x$, and a 50 vol% $Mo/MoSi_x$ microlaminate deposited onto glass cover slips (150 μm thick). The curvature of the cover slip relative to an optical flat was determined before and after deposition by observation in monochromatic light. Curvatures were determined by least squares fitting of parabolas to the recorded fringe spacings and are related to the average stress in the film [6]. All calculations of stress were made using the nominal film thicknesses.

3. Results and discussion

3.1. Coating composition and microstructure

In all the Al_2O_3 films except those at 1000 nm, there is a decrease in the O/Al stoichiometry with increasing R ratio, consistent with observations reported by Shimizu [7] and Kelly [8] for 1 keV Ar^+ bombardment of Al_2O_3 which show a preferential loss of oxygen during bombardment. The oxygen content in

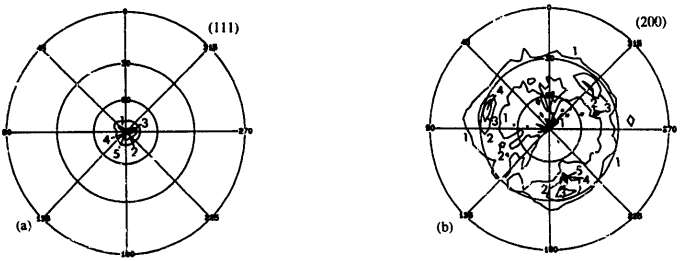

Fig. 1. (111) (a), and (200) (b) pole figures of 1 μm thick Al deposited at $R = 0.1$ (46 eV/atom) using 593 eV Ar^+ at 45° to the substrate normal.

the Al films is relatively constant at about 3 at.% in the films deposited during bombardment. This is about half the value of that incorporated without bombardment (FVD) and is consistent with results of Cuomo et al. [9] who found that ion bombardment of Nb during film growth results in a "cleaning effect" in which the sputter yield ratio of O to Nb approaches 40. Ar incorporation into both Al_2O_3 and Al metal is a function of the R ratio and reaches a value of about 4 at.% at $R = 0.1$.

In Mo films, there is a decrease in the oxygen content with increasing R ratio from 17 at.% (PVD) to 5 at.% ($R = 0.1$), in agreement with results of Cuomo et al. [9]. Ar entrapment remained low, amounting to only 1 at.% at the highest R ratio, also consistent with measurements on Nb [9]. The Si/Mo ratio of the silicide ranged between 1.22 and 1.35, considerably below the target value of 2.0. This may be due to the shape of the Mo plume during deposition caused by uneven melting of the charge material. The Si/Mo ratio decreased with increasing R ratio indicating preferential sputtering of Si, in agreement with results of Liau et al. [10] for PtSi. The oxygen concentration remained low in $MoSi_x$, and tended to decrease with increasing R ratio. The Ar concentration was significantly higher in $MoSi_x$ than in Mo metal which is consistent with observations of greater incorporation of Ar in amorphous materials [11].

The PVD ($R = 0$) Al film displayed a strong (111) fiber texture which was enhanced with increasing R ratio, fig. 1a. The numbers on the pole figures refer to relative X-ray intensities. The (200) pole figure of the PVD sample showed a strong azimuthal orientation, presumably influenced by the single crystal Si substrate. With increasing R ratio, this azimuthal texture was gradually superseded in favor of a different azimuthal texture, fig. 1b, which is also consistent with planar channeling of the ions along (220) planes ((220) pole figure not shown). Recent observations of Dietz et al. [12] showed that a normalized energy of 80 eV/atom is needed to observe a channeling texture in Al. The effect of ion bombardment at lower values of E_n is

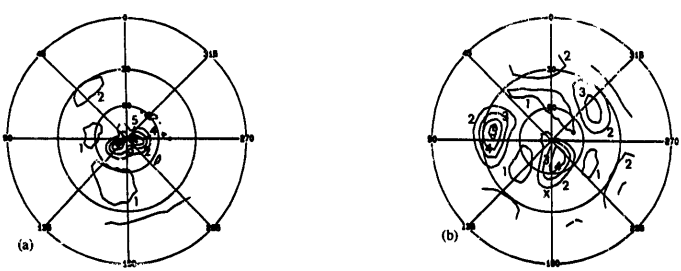

Fig. 2. (110) pole figure of 1.1 μm thick Mo films deposited at (a) $R = 0$ (PVD), and (b) $R = 0.1$ (46 eV/atom) using 500 eV Ar^+ at 45° to the substrate normal.

primarily to increase atomic mobility, allowing more complete development of the preferred growth texture. Their observations are generally consistent with ours except that we observed the development of a channeling texture at 46 eV/atom. Alumina and silicide films were amorphous over all R ratios.

The (110) pole figure for the 1 μm, PVD Mo film, fig. 2a, showed a strong (110) fiber texture perpendicular to the film surface, consistent with the growth texture of bcc films [13]. The pole figure for the 1 μm, $R = 0.1$ Mo film, fig. 2b, indicated a strong (110) fiber texture at an angle of 15° to the substrate, as well as a distinct azimuthal texture represented by the areas of high intensity 60 radial degrees from the fiber axis. The evolution of the azimuthal texture is indicative of planar channeling of the ion beam along (110) planes in the film, resulting in a preferred orientation of the grains along the ion beam direction [13,14]. This channeling behavior is indicated by the high intensity areas located 90° to the ion beam direction. The tilt in the fiber axis is not well understood but correlates with the beam direction.

TEM of planar and cross section samples revealed that the PVD Al films consist of columnar grains extending through the thickness of the sample (1000 nm), fig. 3. Grain diameters are 0.3–0.5 times the length. The size of the grains indicates that the film temperature during deposition was probably less than 200°C [15]. Ion bombardment with an R ratio of 0.04 showed a predominantly columnar structure with a dispersion of finer grains, principally at the film–substrate interface, fig. 3. The grain size changes from about 0.5 μm (PVD) to 0.2 μm ($R = 0.1$). These results suggest that ion bombardment during deposition is increasing the nucleation density, and is most effective at the substrate–film interface.

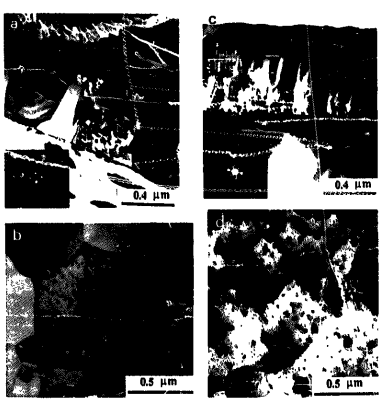

Fig. 3. Bright field electron micrographs (planar and cross section) of 1 μm thick Al films for $R = 0$ (PVD) (a, b), and $R = 0.04$ using 488 eV Ar^+ (c, d).

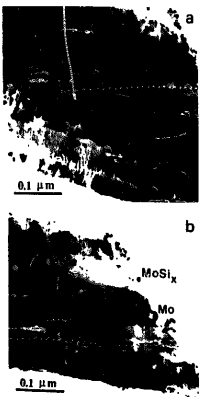

Fig. 4. Bright field electron micrographs of cross sections of 1.1 μm thick Mo/MoSi$_x$ films (a) $R = 0$ (PVD) and (b) $R = 0.07$ for Mo layers and $R = 0.01$ for MoSi$_x$ layers.

Bright field transmission electron micrographs from cross sections of Mo/MoSi$_x$ multilayers deposited by PVD and IBAD are shown in fig. 4. The microstructure shows a fine grain structure for the Mo phase (< 10 nm) and a textureless but "streaked" structure for the silicide phase. The streaking is most likely due to density variations caused either by cracking or the formation of voids. There is little difference between the PVD and IBAD microstructures except that in the IBAD microlaminate, the streaking is less pronounced. These observations are consistent with those of Harper et al. for Nb deposition [14].

3.2. Residual stress

Fig. 5 shows the variation of the average film stress for Mo, MoSi$_x$ and 50 vol% Mo/MoSi$_x$ microlaminate as a function of the normalized energy E_n. The stress in the metal film starts out tensile (0.33 GPa at $E_n = 0$), increases to a peak of 0.63 GPa at $E_n \sim 9$ eV/atom, and becomes compressive at $E_n \sim 30$ eV/atom. The stress of the PVD film ($R = 0$) is in agreement in both sign and magnitude with Nb films deposited in a similar manner by Yee et al. [11]. Since the relative magnitudes of the coefficients of thermal expansion for Mo and the cover slip dictate a compres-

sive stress, the measured tensile stress must be primarily intrinsic in nature. The initial rise in tensile stress and the stress reversal are consistent with the model by Müller [16] in which the rise in tensile stress is believed to be due to the removal of open porosity in the film resulting in a porous, but compact network in which the short range attractive interatomic forces across small defects can act most effectively. These results are also consistent with the idea of a critical film thickness at which the tensile stress increases abruptly due to interconnection of the growing nuclei [17]. Further increases in E_n continue to densify the film forcing the stress toward zero. The compressive stress at higher values of E_n is probably due to point defect production by irradiation damage. Although oxygen incorporation and Ar entrapment have been suggested as possible causes for residual stress changes [18], neither is able to account for the observed behavior of the Mo films.

The silicide and alumina films, figs. 5 and 6, behave very differently from the metal films in that the stress decreases at a very low value of E_n, crosses into the compressive range earlier, and saturates by 15 eV/atom. The immediate decrease in stress and the lower crossover values of E_n may be related to the lower value of the activation energy for self-diffusion in an amorphous structure as compared to a crystalline lattice. Yee et al. [11] found that the R ratio required to cause a transition from tensile to compressive stress was as much as a factor of 3 smaller for amorphous WSi_2 than for crystalline Nb. The saturation in the value of the compressive stress with increasing R ratio is expected for an amorphous structure where the mechanism is due to densification of the microstructure and not the introduction of lattice defects. The higher atom mobility in the amorphous structure may result in more rapid densification causing the elimination of the tensile stress peak, or an effective shift of the curve to lower values of E_n. An alternative explanation for the change in film stress is the entrapment of Ar. The form of Ar in the film is not known, but if it were in solution, then a residual compressive stress would be expected. However, if Ar entrapment was responsible for the compressive stress, then the stress should continue to become more compressive with E_n rather than saturating as observed. Results for multilayer films consisting of five bilayers of 50 vol% Mo and 50 vol% $MoSi_x$ are also shown in fig. 5. The point marked by the arrow designates a film synthesized using $R = 0.07$ for the Mo layers and $R = 0.01$ for the $MoSi_x$ layers corresponding to the crossover points for the pure constituents. Although the residual stresses in the composite do not obey a direct superposition of the stresses of the individual layers, the same trend is evident.

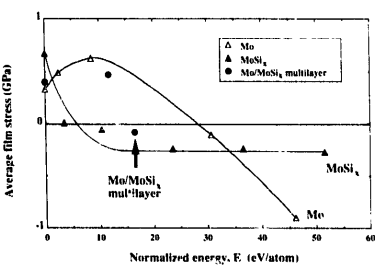

Fig. 5. Average film stress as a function of the normalized energy for 200 nm thick Mo and $MoSi_x$ films and a 1.1 μm thick microlaminate of Mo/$MoSi_x$.

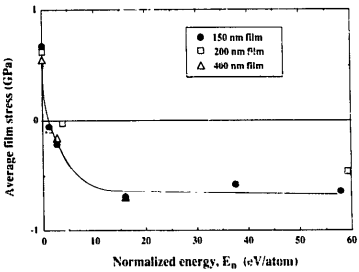

Fig. 6. Average film stress as a function of the normalized energy for Al_2O_3 samples of nominal thickness 150, 200 and 400 nm.

4. Conclusions

Ion beam assisted deposition of Al, Al_2O_3, Mo and $MoSi_x$ using 209–293 eV Ar^+ ions was found to strongly affect the composition, microstructure, texture and residual stress.

- Increasing R ratio leads to an increase in Ar entrapment and a reduction in oxygen incorporation in all films. In Al_2O_3 and $MoSi_x$ films, the stoichiometry becomes increasingly rich in the metallic specie due to preferential sputtering of the light element.
- The (111) fiber texture of deposited Al is intensified with ion bombardment and an azimuthal texture induced by planar channeling along (220) planes develops at higher R ratios. The (110) fiber texture of deposited Mo is intensified with ion bombardment and an azimuthal texture develops due to planar channeling of the ion beam along (110) planes in the film.

- Ion bombardment during deposition results in a breakup of the columnar grain structure and a reduction in grain size in Al films, but produces little visible change in the Mo layers except for a decrease in contrast variations in the silicide layers, presumably due to densification.
- Residual stress in Al_2O_3, $MoSi_x$ and Mo films, and a 50 vol% $Mo/MoSi_x$ microlaminate changes from tension to compression with increasing normalized energy, probably due to ion beam induced densification of the film.

Acknowledgements

The authors sincerely acknowledge The Michigan Ion Beam Laboratory for Surface Modification and Analysis for the use of the IBAD facilities and the Electron Microbeam Analysis Laboratory. This work was supported under NSF grant no. DMR-9100361 and under the Air Force Office of Scientific Research, University Research Initiative Program, contract no. DOD-G-AFOSR-90-0141, Dr. Alan H. Rosenstein, Program Director.

References

[1] A.T. Alpas, J.D. Embury, D.A. Hardwick and R.W. Springer, J. Mater. Sci. 25 (1990) 1603.
[2] D. Tench and J. White, Metall. Trans. 15A (1984) 2039.
[3] T.C. Lu, A.G. Evans, R.J. Hecht and R. Mehrabian, Acta Metall. 39 (1991) 1853.
[4] F.A. Smidt, Int. Mater. Rev. 35 (1990) 61
[5] L.R. Dolittle, Nucl. Instr. and Meth. B9 (1985) 334.
[6] J.A. Thornton, J. Tabock and D.W. Hoffman, Thin Solid Films 64 (1979) 111.
[7] R. Shimizu, Nucl. Instr. and Meth. B18 (1987) 486.
[8] R. Kelly, ibid., p. 388.
[9] J.J. Cuomo, J.M.E. Harper, C.R. Guarnieri, D.S. Yee, L.J. Attanasio, J. Angilelio and C.T. Wu, J. Vac. Sci. Technol. 20 (1982) 349.
[10] Z.L. Liau, J.W. Mayer, W.L. Brown and J.M. Poate, J. Appl. Phys. 49 (1978) 5295.
[11] D.S. Yee, J. Floro, D.J. Mikalsen, J.J. Cuomo, K.Y. Ahn, and D.A. Smith, J. Vac. Sci. Technol. A3 (1985) 2121.
[12] V. Dietz, P. Ehrhart, D. Guggi, H.-G. Haubold, W. Jäger, M Prieler and W. Schilling, Surf. Coat. Technol. 43/44 (1990) 963.
[13] L. See, J.M.E. Harper, J.J. Cuomo and D.A. Smith, J. Vac. Sci. Technol. A4 (1986) 443.
[14] J.M.E. Harper, D.A. Smith, L.S. Yu and J.J. Cuomo, in: Beam–Solid Interactions and Phase Transformations, eds. H. Kurz, G.L. Olsen and J.M. Poate, Mater. Res. Soc. Symp. Proc. 51 (1986) p. 343.
[15] C.R.M. Grovenor, H.T.G. Hentzell and D.A. Smith, Acta. Metall. 32 (1984) 773.
[16] K.-H. Müller, J. Appl. Phys. 62 (1987) 1796.
[17] R.W. Hoffman, in: Physics of Thin Films, eds. G. Hass and R.E. Thun (Academic Press, New York, 1966) p. 230.
[18] T. Wu, J. Vac. Sci. Technol. 20 (1982) 349.